

Off-axis electron holography of Néel-type skyrmions in multilayers of heavy metals and ferromagnets

Supplementary Information

T. Denneulin^{1*}, J. Caron¹, M. Hoffmann², M. Lin³, H.K. Tan^{3,4}, A. Kovács¹, S. Blügel²,
R.E. Dunin-Borkowski¹

¹ *Ernst Ruska-Centre for Microscopy and Spectroscopy with Electrons and Peter Grünberg Institute, Forschungszentrum Jülich, 52425 Jülich, Germany.*

² *Peter Grünberg Institute and Institute for Advanced Simulation, Forschungszentrum Jülich, 52425 Jülich, Germany.*

³ *Institute of Materials Research and Engineering, Agency for Science, Technology and Research (A*STAR), 138634 Singapore.*

⁴ *Data Storage Institute, Agency for Science, Technology and Research (A*STAR), 138634 Singapore.*

**Email address: t.denneulin@fz-juelich.de (T. Denneulin)*

Supplementary Note 1: Influence of out-of-plane and in-plane magnetic moments on phase images of Néel-type skyrmions

The origin of phase contrast recorded from a Néel-type skyrmion in the TEM is generally attributed to the projection of tilted out-of-plane magnetic moments from the core and the external region of the skyrmion. In-plane moments at the skyrmion wall do not lead to phase variations when they are oriented perpendicular to the incident electron beam direction. However, this is no longer the case when the skyrmion is tilted. Figure S1(a) shows a schematic diagram of the projected magnetization when the sample is tilted. In projection, the in-plane magnetization vectors that are oriented perpendicular to the tilt axis are shorter than those oriented parallel to the tilt axis.

Figures S1(b-g) show the influence of the in-plane and out-of-plane components of the magnetic field separately. Figures S1(b-d) show simulations of the total, out-of-plane and in-plane components of the magnetization field, respectively, for a single Néel-type skyrmion. Figures S1(e-g) show phase images calculated from (b-d) at a specimen tilt angle of 20° . As described in the main article, the out-of-plane component (f) results in opposite phase ramps in the core and the external region of the skyrmion. The in-plane component (g) has a quadrupole-like pattern, with two positive and two negative regions. However, these variations are an order of magnitude weaker than those of the out-of-plane plane field. (Note that the range of the color scale is different in (f) and (g)). The total phase image (e) is dominated by the out-of-plane contribution.

In principle, the phase variations related to the in-plane component can be isolated by averaging two phase images obtained at two opposite specimen tilt angles [1]. This would allow the direction of the in-plane moments and hence the skyrmion chirality to be identified. This idea was tested experimentally, however it was not possible to retrieve the weak signal of the in-plane component because of the noise.

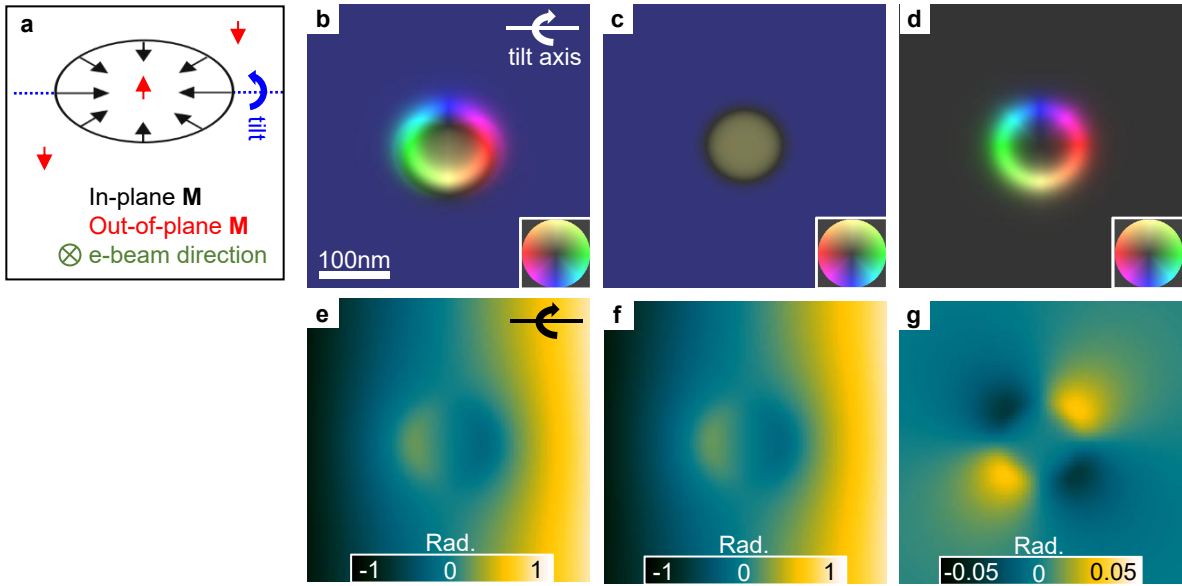


Figure S1: (a) Schematic diagram showing the projected magnetization field of a Néel-type skyrmion when the sample is tilted with respect to the electron beam direction. (b) Simulated total magnetization field of a single Néel-type skyrmion with a tilt angle of 20° . (c) Contribution from the out-of-plane component of the magnetization field in the core and external region of the skyrmion. (d) Contribution from the in-plane component of the magnetization field at the wall of the skyrmion. (e-g) Electron optical phase images calculated from (b-d).

Supplementary Note 2: Influence of bending deformations of the membrane on the domain density in the presence of an applied magnetic field

Figure S2 shows a Fresnel defocus image of the $14 \times [\text{Pt}(1\text{nm})/\text{Co}(0.8\text{nm})/\text{Fe}(0.2\text{nm})/\text{Ir}(1\text{nm})]$ multilayer specimen recorded at low magnification at a nominal specimen tilt angle of -40° in the presence of an applied magnetic field of 194 mT. Micrometer-scale long-range variations in contrast are related to bending deformations of the membrane. Nanometer-scale variations in contrast are associated with magnetic snake-like domains and skyrmions. It can be noticed that the local density of domains changes with these bending deformations of the membrane. For instance, the domain density is higher in the darker regions than in the brighter regions. A possible explanation for this difference is that the inclination of the sample with respect to the applied field direction is higher in the darker regions than in the brighter regions. The out-of-plane component of the external field is then weaker in the darker regions and a stronger applied magnetic field is needed to reach saturation.

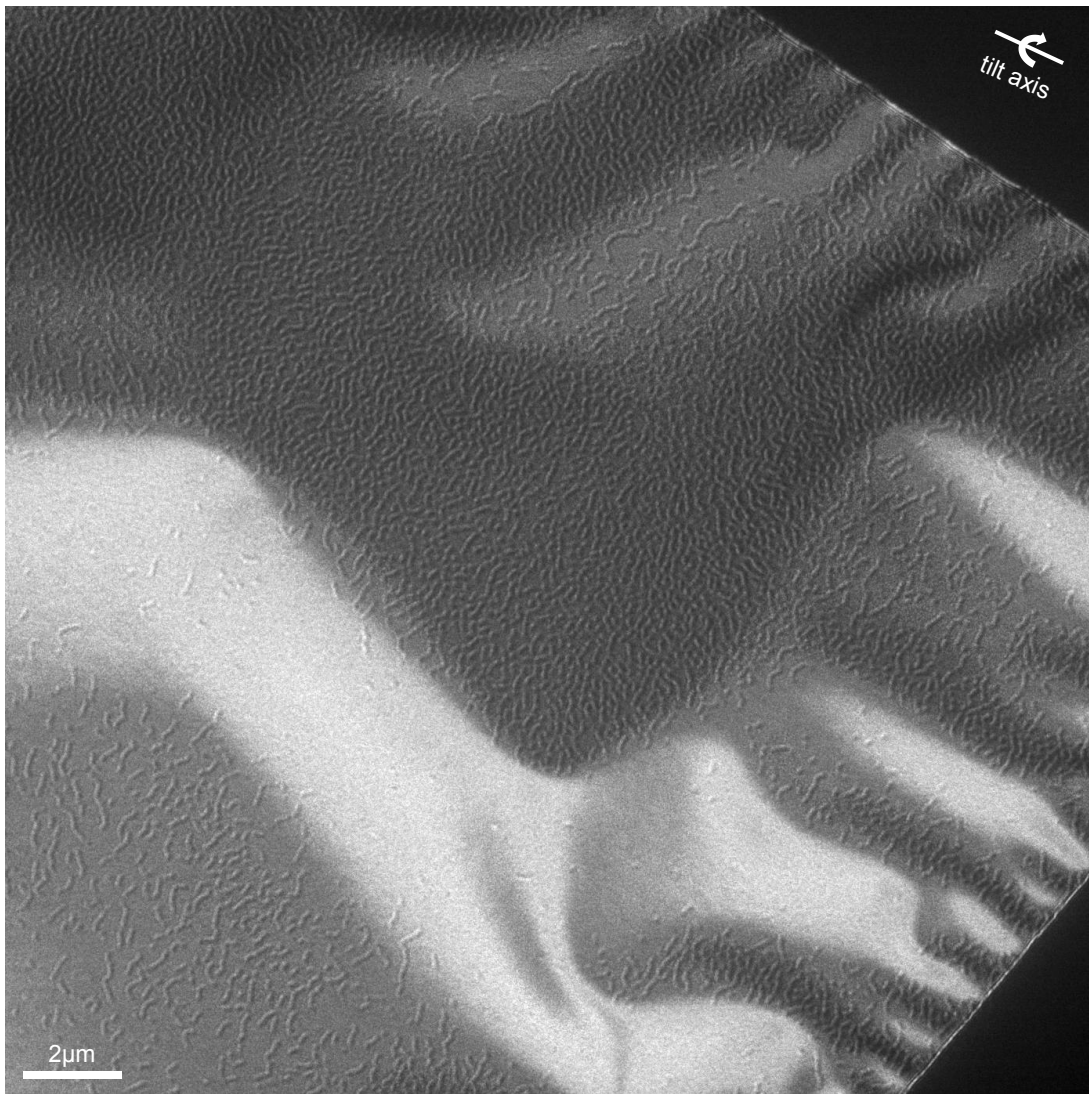


Figure S2: Fresnel defocus image of the $14 \times [\text{Pt}(1\text{nm})/\text{Co}(0.8\text{nm})/\text{Fe}(0.2\text{nm})/\text{Ir}(1\text{nm})]$ multilayer sample with a field of view of approximately $20 \times 20 \mu\text{m}^2$, recorded at a nominal specimen tilt angle of -40° at a defocus of -6 mm in the presence of an applied magnetic field of 194 mT.

Supplementary Note 3: Skyrmion contrast at zero specimen tilt angle

Figure S3(a) shows a tilt series of Fresnel defocus images of individual snake-like magnetic domains and skyrmions in the presence of an applied magnetic field of 161 mT. Local bending deformations of the membrane can modify the orientation of the sample with respect to the incident electron beam direction. (See main article and previous section). Here, care was taken to select a region in which the orientation of the membrane corresponds to the nominal orientation of the specimen stage (*i.e.*, where the magnetic contrast is minimum at 0°). Figure S3(b) shows intensity profiles extracted along the arrows shown in (a) across a snake-like domain at three different specimen tilt angles. The intensities of the profiles obtained at $+20^\circ$ and -20° is inverted and the amplitude of the variation is nearly the same in absolute terms, indicating that the orientation is correct. The image and profile obtained at 0° show almost no magnetic contrast. The absence of contrast at 0° is an indication of the Néel-type texture of the magnetic domains and skyrmions. The presence of a Bloch-type component would result in significant contrast at 0° [2].

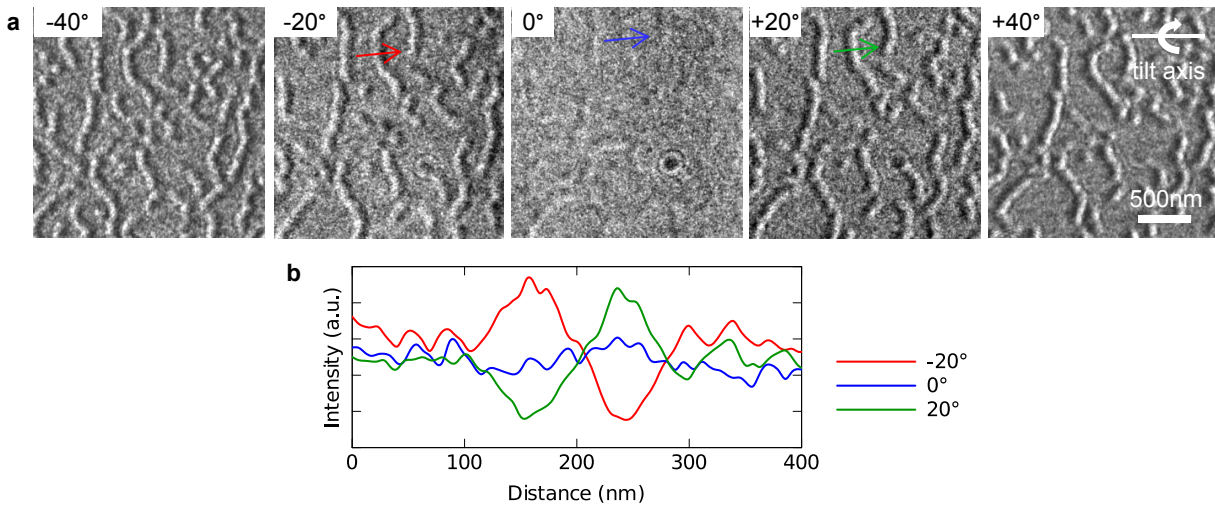


Figure S3: (a) Fresnel defocus images recorded at a defocus of -6 mm at the indicated specimen tilt angles in the presence of an applied magnetic field of 161 mT. (b) Intensity profiles extracted perpendicular to a snake-like domain along the arrows marked in (a) at three different specimen tilt angles.

Supplementary Note 4: Adjustment of the phase ramp using a vacuum region

Figure S4(a) shows an off-axis electron hologram that includes the sample in the top half and vacuum in the bottom half. Figures S4(b, c) show the reconstructed raw phase and the unwrapped phase, respectively. The overall phase ramp was adjusted to minimize phase variations in the vacuum region. The phase shows a horizontal gradient in the sample, increasing from the left to the right side, resulting from the projection of the out-of-plane component of the magnetic field. Additional phase ramps visible near the edge of the hole in (b), over a distance of approximately 300 nm from the specimen edge, may be attributed to damage introduced by the ion beam used to cut the membrane (amorphization, redeposition of particles and thickness variations). This region is masked in (c) because it introduces artifacts in the phase unwrapping algorithm. Figure S4(d) shows a phase profile extracted across the individual skyrmion marked by a red arrow in (c). The phase gradient at the skyrmion core (blue region in (d)) is nearly opposite to that in the outer region as a result of the anti-parallel alignment of the spins in the two regions. The magnetic induction map and phase contour map shown in Figs S4(e, f) confirm that the magnetic field is oriented in opposite directions at the skyrmion core and the outer domain (upwards and downwards, respectively).

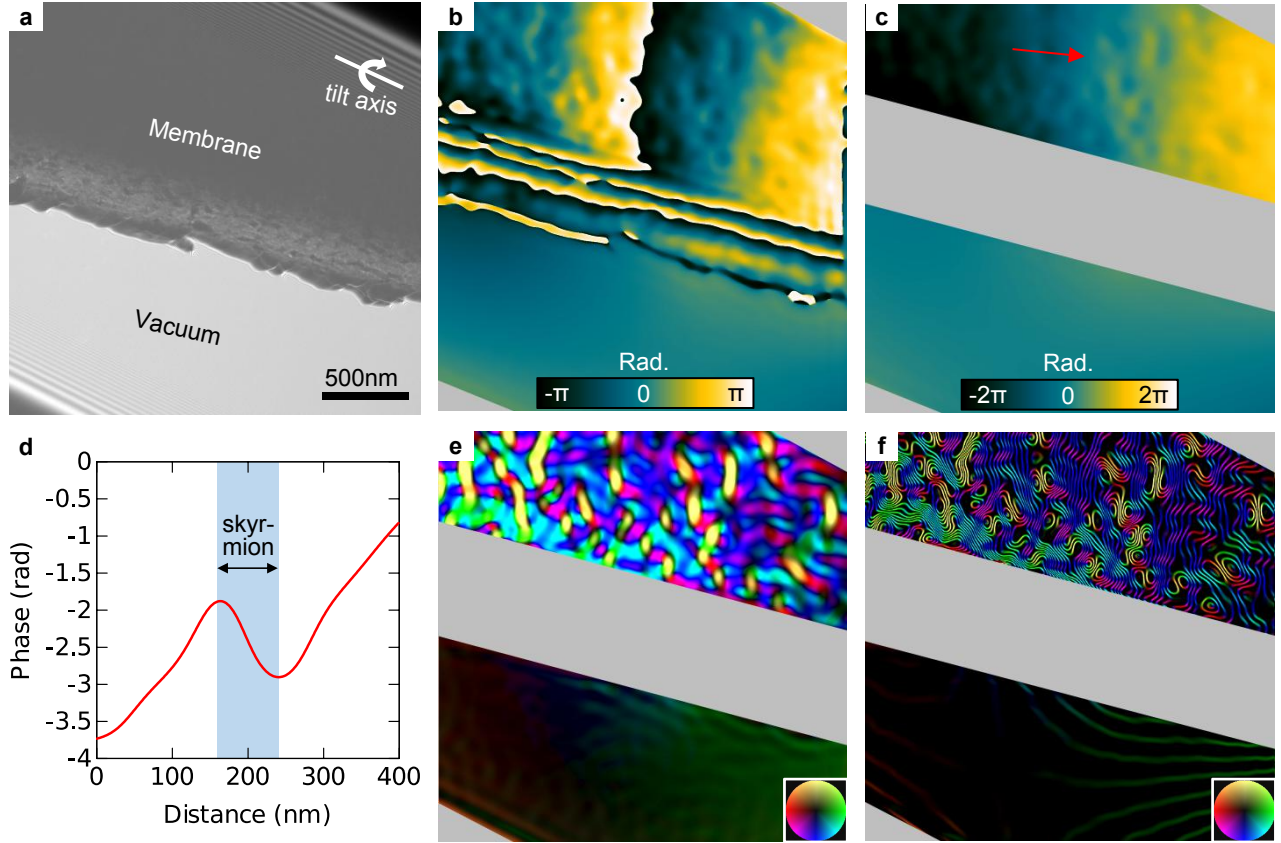


Figure S4: (a) Off-axis electron hologram recorded at a specimen tilt angle of -30° in the presence of an applied magnetic field of 140 mT. A vacuum region is present in the lower part of the hologram. (b) Phase image reconstructed from the hologram shown in (a) using Fourier processing. The overall phase wedge was adjusted to minimize the variations in the vacuum region. (c) Corresponding unwrapped phase image. The region close to the specimen edge has been masked because it introduces artifacts in the phase unwrapping algorithm. (d) Phase profile across a single Néel-type skyrmion extracted along the red arrow marked in (c). The blue area delimited by the peak and the dip in the phase profile corresponds to the diameter of the $M_z = 0$ contour of the skyrmion magnetization. (e) Magnetic induction map and (f) phase contour map (with a contour spacing of $\pi/30$ rad) calculated from the gradient of the phase image. The direction of the projected in-plane component of the B field is given by the color wheel at the lower right corner.

Supplementary Note 5: Measurement of magnetic domain wall width

Figure S5(a) shows a phase image of snake-like magnetic domains recorded in the presence of an applied magnetic field of 65 mT at a specimen tilt angle of -15° . A large mask was used in Fourier space to optimize the spatial resolution, which is approximately 10 nm (*i.e.*, approximately three times the hologram interference fringe spacing). The snake-like magnetic domains are oriented preferentially in a direction perpendicular to the specimen tilt axis, *i.e.*, along the direction of the applied magnetic field. The image was rotated so that the elongation direction of the domains corresponds with the vertical axis of the image. Figure S5(b) shows the gradient of the phase calculated in the horizontal direction. The phase gradient is proportional to the vertical component of the magnetic induction field projected in the image plane. Figure S5(c) shows a phase gradient profile extracted across an individual snake-like magnetic domain corresponding to the red box marked in (b), in a direction perpendicular to the domain walls. In order to reduce noise, the profile was averaged in the vertical direction (parallel to the domain walls) over a distance of 250 nm. The profile was then fitted using two \tanh functions, as shown in Fig. S5(c). The functions are defined by the expression $y = y_0 + a \tanh((x - x_0)/w)$ where y_0 , a , x_0 and w are constants obtained from the fit. For both the left and the right domain wall, the fit converges when $w = 7$ nm. The width of the domain wall can then be defined as $\pi w = 21 \text{ nm} \pm 10 \text{ nm}$ (where the uncertainty corresponds to the spatial resolution). The positions of the domain walls (DW) are indicated using gray rectangles on the plot.

For comparison, the width parameter w can be calculated using the expression $w = \sqrt{(A/K_{\text{eff}})}$, where K_{eff} is the magnetic anisotropy and A is the exchange stiffness [3]. Based on a previous study on similar samples [4], it can be estimated that $K_{\text{eff}} \approx 0.2 \text{ MJ.m}^{-3}$ and $A \approx 12 \text{ pJ.m}^{-1}$. It gives $w = 8 \text{ nm}$, which is in very good agreement with the parameter determined experimentally.

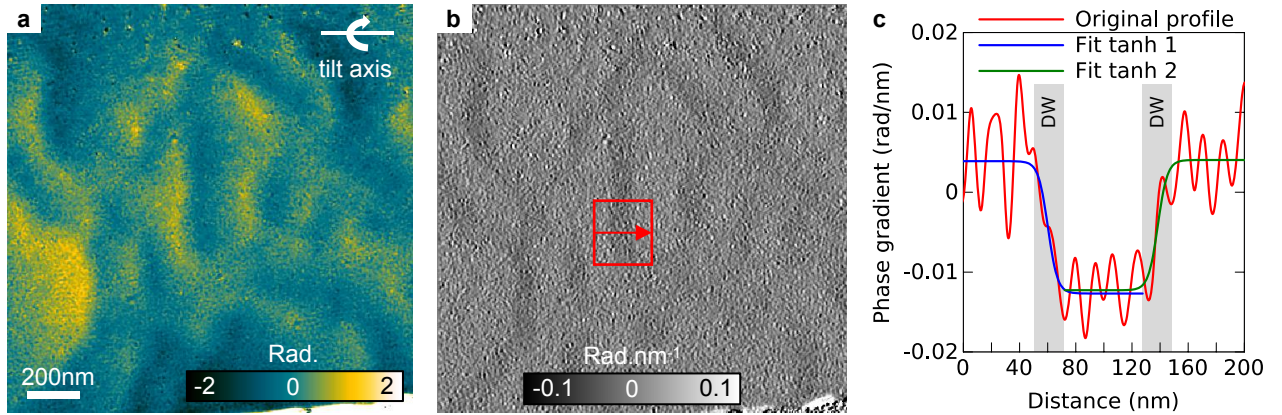


Figure S5: (a) Phase image of snake-like magnetic domains recorded at a specimen tilt angle of -15° in the presence of an applied magnetic field of 65 mT. The spatial resolution of the phase image is approximately 10 nm. (b) Phase gradient of (a) calculated in the horizontal direction. (c) Line profile extracted from (b) across an individual snake-like domain at the position of the red box. The profile was averaged over 250 nm in a direction parallel to the domain walls and fitted using two \tanh functions. Gray rectangles mark the positions of the domain walls (DW).

References

- [1] W. Jiang, S. Zhang, X. Wang, C. Phatak, Q. Wang, W. Zhang, M. B. Jungfleisch, J. E. Pearson, Y. Liu, J. Zang, X. Cheng, A. Petford-Long, A. Hoffmann, S. G. E. te Velthuis, Quantifying chiral exchange interaction for Néel-type skyrmions via Lorentz transmission electron microscopy, *Physical Review B* 99 (2019) 104402. doi:10.1103/PhysRevB.99.104402.
URL <https://link.aps.org/doi/10.1103/PhysRevB.99.104402>
- [2] M. J. Benitez, A. Hrabec, A. P. Mihai, T. A. Moore, G. Burnell, D. McGrouther, C. H. Marrows, S. McVitie, Magnetic microscopy and topological stability of homochiral Néel domain walls in a Pt/Co/AlO_x trilayer, *Nature Communications* 6 (2015) 8957. doi:10.1038/ncomms9957.
URL <https://www.nature.com/articles/ncomms9957>
- [3] D. C. Jiles, *Introduction to Magnetism and Magnetic Materials*, 3rd Edition, CRC Press, 2015. doi:10.1201/b18948.
URL <https://www.taylorfrancis.com/books/9780429160097>
- [4] A. Soumyanarayanan, M. Raju, A. L. Gonzalez Oyarce, A. K. C. Tan, M.-Y. Im, A. P. Petrović, P. Ho, K. H. Khoo, M. Tran, C. K. Gan, F. Ernult, C. Panagopoulos, Tunable room-temperature magnetic skyrmions in Ir/Fe/Co/Pt multilayers, *Nature Materials* 16 (2017) 898. doi:10.1038/nmat4934.
URL <https://www.nature.com/articles/nmat4934>